Published in IEEE Transactions on Electromagnetic Compatibility, vol. 65, no. 1, pp. 281-291, Feb. 2023, doi: 10.1109/TEMC.2022.3217393

Validation of Lightning Simulation compared with measurements using DCI technique post-processed to be applied to a lightning threat

Guadalupe Gutiérrez, Raúl Molero, Hugo Tavares, Hirahi Galindo, Enrique Pascual Gil, *Member, IEEE*, Miguel R. Cabello, Salvador González García, *Senior Member, IEEE*

***Abstract*— The Direct Current Injection (DCI) technique is a complicated method which involves both a testing campaign and electromagnetic simulations. Consequently, it takes a long time, entails high costs, and requires a lot of effort in a complex post-process. The present paper shows that only with the lightning simulations, also involved in the DCI process, similar and useful information can be obtained. Currents induced on cables in a lightning simulation on an aircraft cockpit are compared with the post-processed results coming from a low-level DCI test, demonstrating good agreement within the established margin, and analyzing the identified differences. This example illustrates the benefits of using simulations in reducing costs and delivery time. We also show their potential benefit in improving the aircraft safety by using them from the earlier stages of the design to the end of service of the aircraft. This is achieved thanks to their capability to predict the behavior of the object in configurations which could not be addressed by test, and by checking a larger number of probes, which could even be placed in non-accessible areas.**

***Index Terms*—Lightning simulation, DCI, validation.**

I. INTRODUCTION

IN aeronautics, the lightning event is characterized by a high level current injected on the aircraft structure when a lightning strike impacts the aircraft. This phenomenon can damage the structure itself, as well as for the on-board equipment, and it has the potential to disturb the normal operation of electrical and electronic equipment. When the lightning current flows through the aircraft skin, strong and time-varying magnetic fields are produced, whose effects dominate over the electric field ones at low-frequency. The magnetic flux may leak inside the aircraft through apertures or be diffused inside through composite exterior surfaces. Then, the internal magnetic fields couple to the electrical wiring, resulting in a common-mode induced voltage proportional to the rate of change of the magnetic field, and to the area of the loops formed by wires and the ground reference [1].

Among the techniques used to evaluate the lightning protection of an aircraft, one of the most commonly used is the low-level Direct Current Injection (DCI) or Low-Level Direct Drive (LLDD). This measurement technique is used to demonstrate compliance with lightning regulation [2], and also with High-Intensity Radiated Fields (HIRF) regulation in its lower frequency range [3]. Low-level coupling tests (used to determine the internal environment) are the preferred airplane test methods with respect to high-level tests (used to evaluate the effect on the systems) due to the higher test rigor, flexibility, lower-cost, and availability of low-level techniques [3].

The DCI process entails a complicated procedure. This technique is needed from 10 kHz up to around 2 MHz for HIRF certification due to the difficulty of having a good radiating antenna at this lower frequency range, and its results are normally used up to the first resonant frequency of the object. The objective is to find out the currents induced into the cables due to an applied external field by relating, in a first step, these currents with the surface current densities excited in the aircraft skin by measurements. In a second step, the surface current densities excited in the aircraft skin are related to the applied external field by simulations. For large aircrafts, the technique is usually applied using the embedded mesh of the test site floor as the ground plane, or placing some kind of conductors above the floor to ease the current return [4]. However, whenever possible, it is recommended the use of a cage return wire network arranged around the object under test, so as to improve the homogeneity of the surface current distribution and decrease the reflection coefficient, thus reducing the error when extrapolating the measured results to in-flight conditions [2], [3].

The defined DCI process in low-level and also lightning simulations have been applied to an aircraft cockpit manufactured as a hybrid structure composed of metal, carbon fiber composite (CFC), and CFC plus expanded copper foil of

Manuscript received March xx, 2022.

The work described in this paper has received funding from the European Community's H2020-EU.3.4.5.4. | ITD Airframe Programme with Topic CS2-GAM-2018-AIR | Airframes under grant agreement ID 807083, and by the Spanish MICINN, EU FEDER under Project PID2019.106120RB.C33.

(Corresponding author: Salvador González García).

Guadalupe Gutiérrez, Hirahi Galindo and Enrique Pascual Gil are with the Computational Electromagnetics Area at Airbus Defence and Space, 28906 Getafe (Madrid), Spain (guadalupe.gutierrez@airbus.com, hirahi.galindo-perez@airbus.com, enrique.pascual@airbus.com).

Raúl Molero is with the EMC Testing Department at Airbus Defence and Space, 28906 Getafe (Madrid), Spain (raul.molero@airbus.com).

Hugo Tavares is with the Electromagnetic Environmental Effects Department at the Instituto de Soldadura e Qualidade, Oeiras, Portugal (HVTavares@isq.pt).

Miguel Ruiz Cabello and Salvador González García are with the Department of Electromagnetism, University of Granada, Granada, Spain (mcabello@ugr.es, salva@ugr.es).

Color versions of one or more of the figures in this article are available online at http://ieeexplore.ieee.org

175 g/m^2 (ECF175) (see Fig. 1), within the scope of the Passaro project (Clean Sky 2) [5-8]. This cockpit was equipped with a realistic electrical installation including seven metal boxes as dummy equipment and two over-braided harnesses with several inner conductors.

Fig. 1. Test case in DCI set-up.

A complex post-process must be applied to the data obtained using DCI technique so as to use them in a lightning qualification/certification process. The main objective of this paper is to use these post-processed values to validate lightning simulations, proving their usefulness to evaluate the aircraft lightning protection through its whole life cycle.

The paper is organized as follows. In section II, a description of the electromagnetic (EM) model and the physical test case is provided. Section III presents the required mathematical models to handle the problem. In section IV, the lightning simulations performed are explained. Section V describes the low-level DCI test carried out on this test case, detailing the way its results should be post-processed so as to apply it to a lightning indirect effects (LIE) certification. Section VI presents the comparison between the results coming from both lightning simulations and post-processed DCI technique. In section VII, the approval criterion is established. Afterwards, in section VIII, the validation results are discussed. And, finally, section IX summarizes the main conclusions.

II. MODEL DESCRIPTION: PASSARO COCKPIT

An EM model was generated by Airbus Defence and Space (ADS) [9], from the digital mock-up of the cockpit in CATIA [10]. Different properties were assigned to the pieces of the cockpit according to their material composition. However, geometry has been extremely simplified to make it light and manageable, while it assures the necessary contacts between pieces and avoids the unwanted connections [11-14].

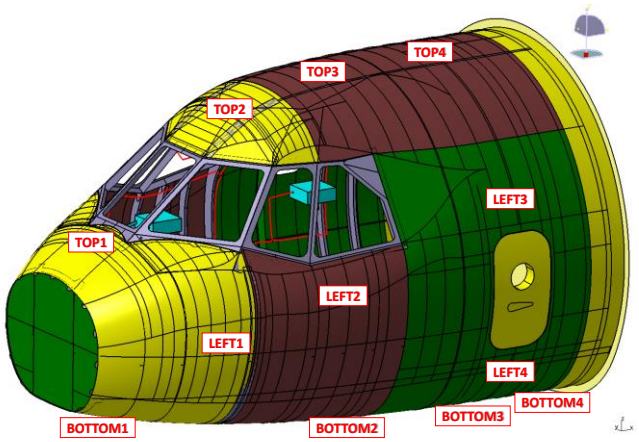

Fig. 2. EM model with surface current density probe locations.

The cockpit is equipped with an electrical installation in order to represent the one of a real aircraft. Two over-braided harnesses are installed, one of them mainly routed along the top half of the cockpit, and other one along the bottom volume below the cockpit floor (which is non-conductive). Each harness has several branches ended at metal boxes as items of equipment, making a total of seven boxes grounded to the structure. Two different over-braid sizes are used on different branches depending on their number of inner conductors and cable routing. Equipment boxes and harnesses were also included in the EM model.

Two kinds of probes are used in the present analysis: sixteen surface current density probes located over the aerodynamic surface of the cockpit at positions made of different materials (see Fig. 2), and ten current probes at every over-braid branch (see Fig. 3). The initial letter L in the current probe names stands for Loom currents. The second letter is T for the Top harness probes and B for the Bottom harness. The third letter B means Box, and following numbers/letters indicate each particular box, except for the LTM probe which corresponds to a cable branch which is not connected to a shielded box but is between two harness junctions.

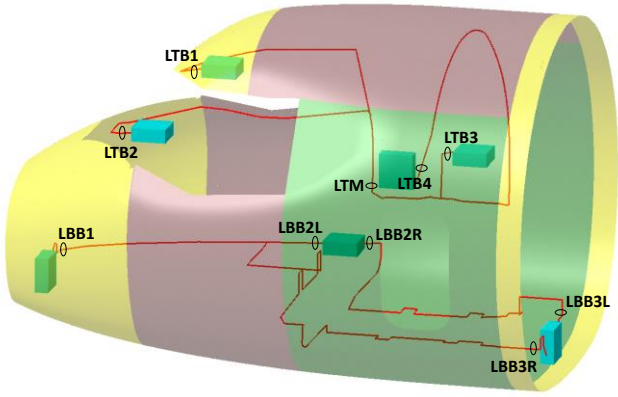

Fig. 3. EM model with cable current probe locations.

A first validation of this EM model directly against measurements was presented in [7]. For that purpose, the test set-up (cage return wire network, injection rig and exit rig) had

to be included in the model.

III. MATHEMATICAL MODELS USEFUL FOR EM SIMULATIONS IN AERONAUTICS

A. Governing Equations

As it is well known, Maxwell curl equations explain the whole phenomenology involved in the problem under study, either directly or by means of approximations (circuital, high-frecuency, etc.). They constitute, in time domain, a hyperbolic set of partial differential equations, relating the electric $\vec{E}$ and magnetic $\vec{H}$ field vectors, function of space and time $\vec{r}$, t, by

$$-\nabla\times\vec{E}=\vec{M}_T+\mu_0\frac{\partial\vec{H}}{\partial t}\quad,\quad\nabla\times\vec{H}=\vec{J}_T+\varepsilon_0\frac{\partial\vec{E}}{\partial t}\quad(1)$$

where ε_0, μ_0 are the free-space permittivity and permeability, and $\vec{J}_T$, $\vec{M}_T$ are the total electric and magnetic current densities. These can in turn be split as

$$\vec{M}_T=\vec{M}_s+\vec{M}\quad,\quad\vec{J}_T=\vec{J}_s+\vec{J}\qquad(2)$$

Where $\vec{J}_s$, $\vec{M}_s$ represent the independent source current densities used as excitation sources (plane waves, dipoles, etc.), and the other $\vec{J}$, $\vec{M}$ are the current densities associated to the physical properties of the materials present in the problem including the electric and magnetic conduction and polarization current densities. These depend, in turn, on the electric and magnetic fields for isotropic linear media in frequency domain, according to

$$\begin{aligned}\vec{J}&=j\omega\left(\varepsilon_0\chi_e(\omega)+\frac{\sigma_e}{j\omega}\right)\vec{E}(\omega)\\\vec{M}&=j\omega\left(\mu_0\chi_m(\omega)+\frac{\sigma_m}{j\omega}\right)\vec{H}(\omega)\end{aligned}\qquad(3)$$

σ_e, σ_m, are the electric and magnetic conductivities, and $\chi_e(\omega)$, $\chi_m(\omega)$ the electric and magnetic susceptibilities of the material (these equations can also be cast as a function of the permittivity and permeability by setting $\varepsilon(\omega)=\varepsilon_0(1+\chi_e(\omega)),\mu(\omega)=\mu_0(1+\chi_m(\omega))$. The frequency domain expressions (3) can be expressed back into time domain either in differential or convolutional form. The way in which it has been employed in the numerical tool used in this paper is based in [15]. For this, the frequency functions $\chi_e(\omega)$, $\chi_m(\omega)$ are first expanded as the sum of an arbitrary-order partial fraction complex (non-degenerate) pole/residue series, found by vector fitting techniques [16]. Next, each single term is transformed into an electric/magnetic current term related to the E/H field by a simple first order ordinary differential equation, and they are summed up to get the total current, together with the conductive terms.

B. Numerical Solution: FDTD

The Finite Difference Time Domain (FDTD) method is probably the most widely used numerical method in computational EM to solve Maxwell equations [17]. For being in time domain, it can predict the wideband response of the system, including in a natural manner any kind of material, source, boundary condition, etc.

However, to simulate the whole complexity of this problem, the FDTD method must be endowed with subcell numerical models to make it computationally affordable. In this paper we employ the SEMBA numerical tool based in FDTD with several enhancements, capable of taking into account the whole EM scenario. SEMBA [18] has been developed by the University of Granada, with contributions from ADS, and has been broadly validated for years [19].

The classical Yee FDTD method [20] employs second-order centered differences to replace all the space/time derivatives in Maxwell's curl equations (as well as the time derivatives in the time-domain constitutive relationships). This kind of discretization, in Cartesian coordinates, requires the space to be sampled in unit cells with space step (Δx, Δy, Δz), in a not necessarily uniform grid, with the EM field-components placed in the well-known Yee's cube staggered spatial arrangement, also staggered in time by a Δt/2 factor. The result is a final discrete explicit marching-on-in-time algorithm, which finds the solution at a given time instant causally as a function of the solution at previous time steps. A common rule of thumb is that a spatial resolution of 15-20 space steps per wavelength at the maximum frequency provides enough accuracy in homogenous materials. However, geometrical fine details actually require space steps small enough to account for their physical size (curvature, thickness, etc.) to sample properly the space variations of fields at and around them.

A main restriction of the marching-on-in-time explicit algorithm is that it requires the time step to be minored by the smallest space step of the spatial mesh to ensure its numerical stability. This is described by the well-known Courant-Friedrichs-Lewy (CFL) criterion, which requires the so-called CFL Number to fulfil in 3D [17].

$$CFLN\equiv\frac{c\Delta t}{\underset{\forall i}{Min}\left\{\left(\sqrt{\frac{1}{\Delta x_i^2}+\frac{1}{\Delta y_i^2}+\frac{1}{\Delta z_i^2}}\right)^{-1}\right\}}\leq 1\qquad(4)$$

Hence, a fine space discretization required to mesh fine details, also imply smaller time steps, and, subsequently, larger simulation times to achieve a physical final time. This becomes critical in slowly converging low-frequency problems, like the ones under study in this work, and we resort to permittivity scaling methods, cited below, to alleviate the situation [21, 22].

Furthermore, the need of dense space meshes to handle both the homogeneous parts of the materials and the fine details arising at the geometrical boundaries between them, lead to huge-memory requirements. Though FDTD is easily implemented in cluster architectures, its main bottleneck is actually the memory bandwidth access [23]. So, a solution to

account for involved transitions (curvatures, cables, gaps, thin panels), better than resorting to a brute-force fine mesh, is to keep the coarse mesh in the homogeneous regions and to use proper sub-cell techniques hybridized with the usual Yee FDTD updating scheme. SEMBA includes the following specific sub-cell models and enhancements, most of them required for the simulations presented in this paper:

• To deal with thin materials, like the CFC skin of an aircraft, Impedance Boundary Conditions (IBC) can be used [24], though we have opted, for its superior stability properties, to use an alternative referred to as Sub-Gridding Boundary Condition (SGBC) technique proposed in [25], which hybridizes a 1D Crank-Nicolson FDTD scheme to deal with the field propagation inside the thin-panel, with the usual 3D Yee-FDTD scheme for the rest of the problem.

• To handle cable bundles, once again brute-force meshing is not the solution. Hence, the thin wire formalism proposed by Holland in [26] has been used.

• Capability to use a permittivity scaling method [21, 22] to speed up the convergence of low frequency transients, which is especially useful in the simulation of lightning problems, where a long transient has to be calculated, the spectral content is limited and the response is analyzed in the time domain.

Finally, in order to simulate open problems, proper reflection-less absorbing boundary conditions are required. Mur boundary conditions [27] are the ones chosen to be used in this work for being accurate in low frequency, and especially suited to simulate current injection (and lightning channel) problems. For this, we employ a line of soft electric sources, with the desired time evolution, connecting the Mur boundary conditions to the entry point at the aircraft (e.g., at the cockpit), and acts as a current injector. In turn, a PEC line runs from the exit point of the currents (e.g., at the tail plane) up to the Mur conditions, permitting to draw the current out of the aircraft.

The SEMBA tool employs the GiD CAD/CAE tool which is an interactive graphical user interface used for the definition, preparation, and visualization of all the data related to a numerical simulation [28]. It employs proprietary conformal meshing tools [29, 30] that search for a trade-off between optimally conforming the original geometry, to overcome the classical stair-casing problem of the finite difference methods, with no dramatic reductions in the time step of stability. SEMBA has been broadly validated with most typical EMC problems of Lightning/HIRF involving complex and electrically large geometries [19, 31-36], and has demonstrated its capability to handle the complexity of problems like the one described in this paper.

IV. LIGHTNING SIMULATION

We have performed Lightning simulations for the configuration with the cockpit in-flight conditions, without any test set-up included in the model but the cockpit in the air, with a lightning channel impacting at the center of the first frame and exiting by the center of the back cover. The model is excited with a Waveform A (WFA) transient [37], and the current induced on every cable branch is calculated.

A Cartesian FDTD mesh with a uniform space-step of 10 mm was employed for the simulations. Mur absorbing boundary conditions of first order were employed to truncate the domain, yielding a problem size of almost 160 Mcells. A time-step of 12 ps was employed to meet the CFL stability condition established in (4). A total time of 500 μs was simulated making use of the permittivity scaling technique to accelerate the calculation.

Non-metallic parts (CFC and CFC+ECF175) have been modeled using SGBC technique to capture the diffusion effect. Average conductivity (σ) and thickness (thk) values equal to σ = 22 kS/m, thk = 2 mm and σ = 330 kS/m, thk = 2 mm have been assigned, respectively.

Theoretical values of resistance per unit length have been applied to every over-braid branch, that is, 3.57 mΩ/m for branches of 10 mm in diameter and 4.59 mΩ/m for branches of 7.5 mm in diameter. Measured values of back-shell connector resistances were employed, ranging from 0.3 to 4 mΩ, due to the connection variability according to their actual installation conditions.

Permittivity scaling method was used to speed up the simulation since WFA is a long waveform with significant content in low frequency. A scaling factor of 10 for the electric field starting at 65% of the waveform time to peak was estimated to be optimum for this particular object and cluster characteristics.

Eventually, the use of conformal meshing was not deemed necessary because the size of the object made it possible to use a cell resolution small enough to represent the geometrical details.

A computation speed of about 2300 Mcells per second in double precision and core was reached in an Intel Xeon Gold 6154 cluster with 18 cores per processor and 2 processors per node of 3.00 GHz frequency and 192 GB RAM memory each node, using Message Passing Interface (MPI) and Open Multi Processing (OpenMP) parallelization methods. The mentioned speed and the permittivity scaling approximation gave us the possibility of finishing the simulation up to 500 μs in 4 days using only 4 nodes of the machine.

V. DCI TECHNIQUE APPLIED TO LIGHTNING

The DCI process is a complicated method which involves both measurements and simulations. There is literature on the application and validity of this technique for HIRF [38-42], and also [35, 36, 43, 44], but no publications have been found by the authors on the application of DCI for lightning.

From the point of view of lightning, the aim of the technique is to know the currents induced in the cabling due to a lightning impact. In this method, the currents induced in the cabling and the surface current density over the object skin due to a current injection which is distributed all over the object are measured on-ground. Besides that, the surface current densities excited in the object skin by a lightning impact in-flight conditions are found by simulation in order to apply an in-flight to on-ground correction factor to the induced current test data [3].

Therefore, the same simulation described in the previous

section (lightning simulation) is used in the DCI technique to calculate, in this case, the surface current density over the cockpit skin.

Using the measured data obtained from the DCI test and the calculated data from the lightning simulation, a complex post-process is needed to get the required results. In this post-process, the currents induced in the cabling with the aircraft in-flight conditions are calculated from the currents induced in the cabling with the aircraft on-ground conditions (test data), applying a correction factor. This correction factor is the relation between the current density on the aircraft skin in-flight conditions (simulated data) and the current density on the aircraft skin on-ground (test data) [3].

This analysis is based on the fact that the skin currents on exterior surfaces induce currents on local cables by magnetic coupling, and the induced cable current is proportional to the local exterior skin current [3]. This proportionality can be expressed in frequency domain by

$$\frac{I_{if}}{J_{if}} = \frac{I_{og}}{J_{og}} \tag{5}$$

where *I* is the current induced on a cable, *J* the surface current density, *if* stands for in-flight and *og* stands for on-ground.
We can introduce a correction factor found by dividing the current density under in−flight conditions normalized to the lightning strike current (here assumed to be the waveform A), I_{WFA}, over the current density on−ground conditions normalized by the injected current, I_{inj},

$$CF = \frac{J_{if}/I_{WFA}}{J_{og}/I_{inj}} \tag{6}$$

to finally yield

$$I_{if} = \frac{I_{og}}{I_{inj}} \cdot CF \cdot I_{WFA} \tag{7}$$

Thus, the current in-flight is determined by the current measured on-ground normalized by the injected current, with the on-ground effect corrected by the correction factor and converted into an in-flight current induced on a cable by the WFA transient.

To this end, a post-process which uses measured and simulated data should be followed. The flowchart shown in Fig. 4 depicts the process. In this flowchart, LIE stands for Lightning Indirect Effects, DCI2LIE for the results obtained in DCI test post-processed to obtain the response to lightning, and DCI2LIE CF to these latest results applying to them the correction factor. The routine described in Fig. 4 has been verified by performing the whole post-process using simulation data for all the variables (currents and current densities both in-flight and on-ground); logically, this approach improves a lot the agreement. Moreover, the routine has also been verified by performing the post-process making use of some measurements carried out in time domain; good agreement has also been obtained. For the sake of simplicity, these results are not presented here because they are out of the scope of the present paper.

In our case we have used a bandwidth of 100 MHz and a frequency step of 1 kHz to construct the desired frequency vector.

Since the cabling is distributed by the whole inner volume of the cockpit, we are going to consider the sixteen surface current density probes to calculate the correction factor (for other objects like an aircraft, only the points over each cable routing should be computed for each particular cable). It must be taken into account that the aim of this study is to perform a validation and not to look for the worst-case on certification purposes, so that the mean value among the sixteen correction factors have been selected instead of their maximum value.

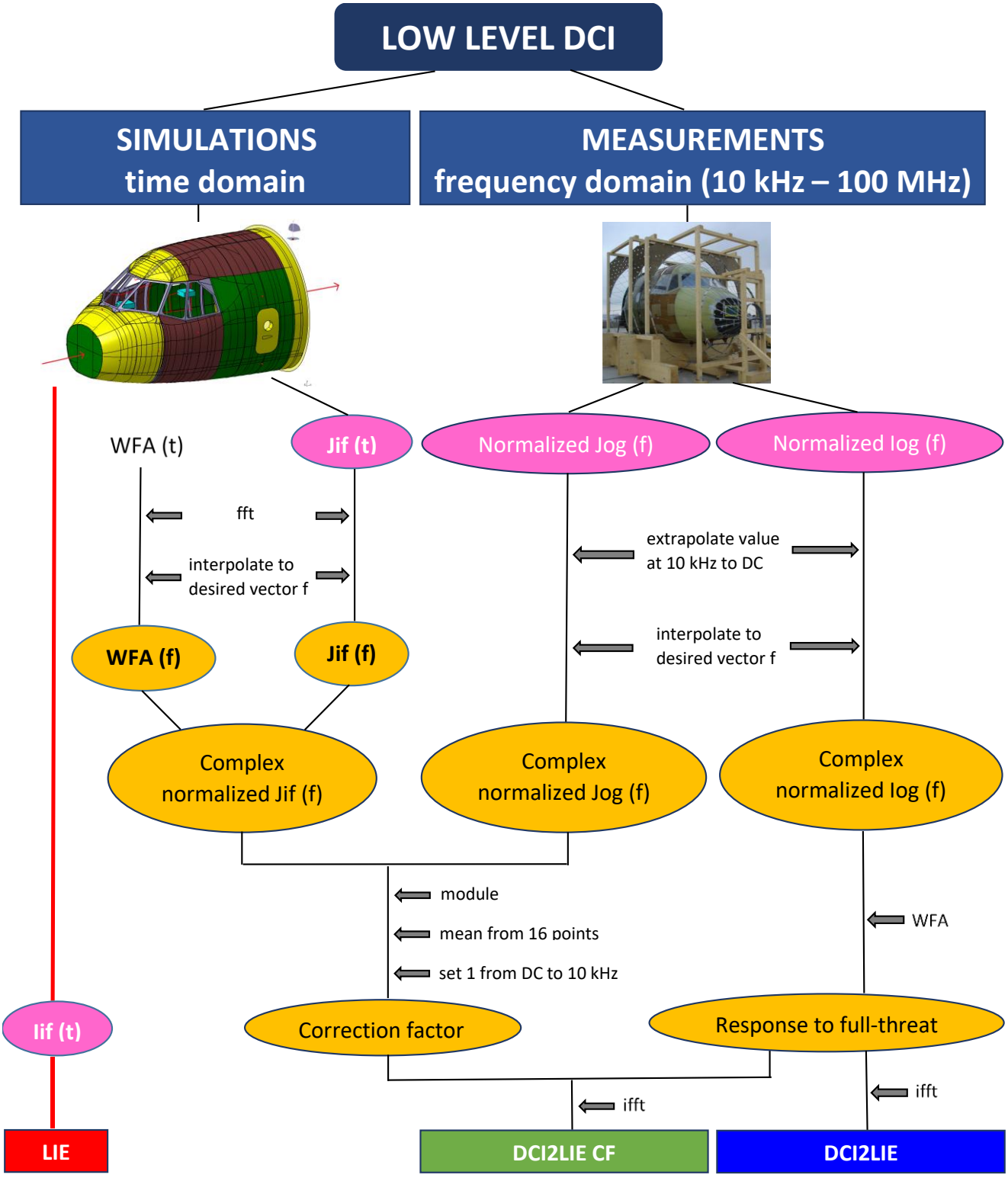

Fig. 4. Post-process flowchart. On the right-hand side, the post-process which should be applied to the measured values is detailed. Going downwards, at a certain level of the post-process, data coming from simulations are needed to introduce the correction factor. Thus, we obtain the results coming from the DCI technique applied to lightning (with and without the application of the correction factor). All this post-process can be shortcut by the red line on the left-hand side, which represents the lightning simulation for obtaining the currents induced in the cabling.

VI. COMPARISON OF RESULTS

These final results are compared to the simulated currents on cables in-flight in Fig. 5. When assessing the similarity between these curves, it must be taken into account what we are comparing. On the one hand, we simply have a lightning simulation, whereas, on the other hand, we have a complex process in which some measurements have been corrected by a factor coming from other measurements and simulations using a data processing which offers many possibilities. Moreover, the curves are compared in linear magnitude versus time.

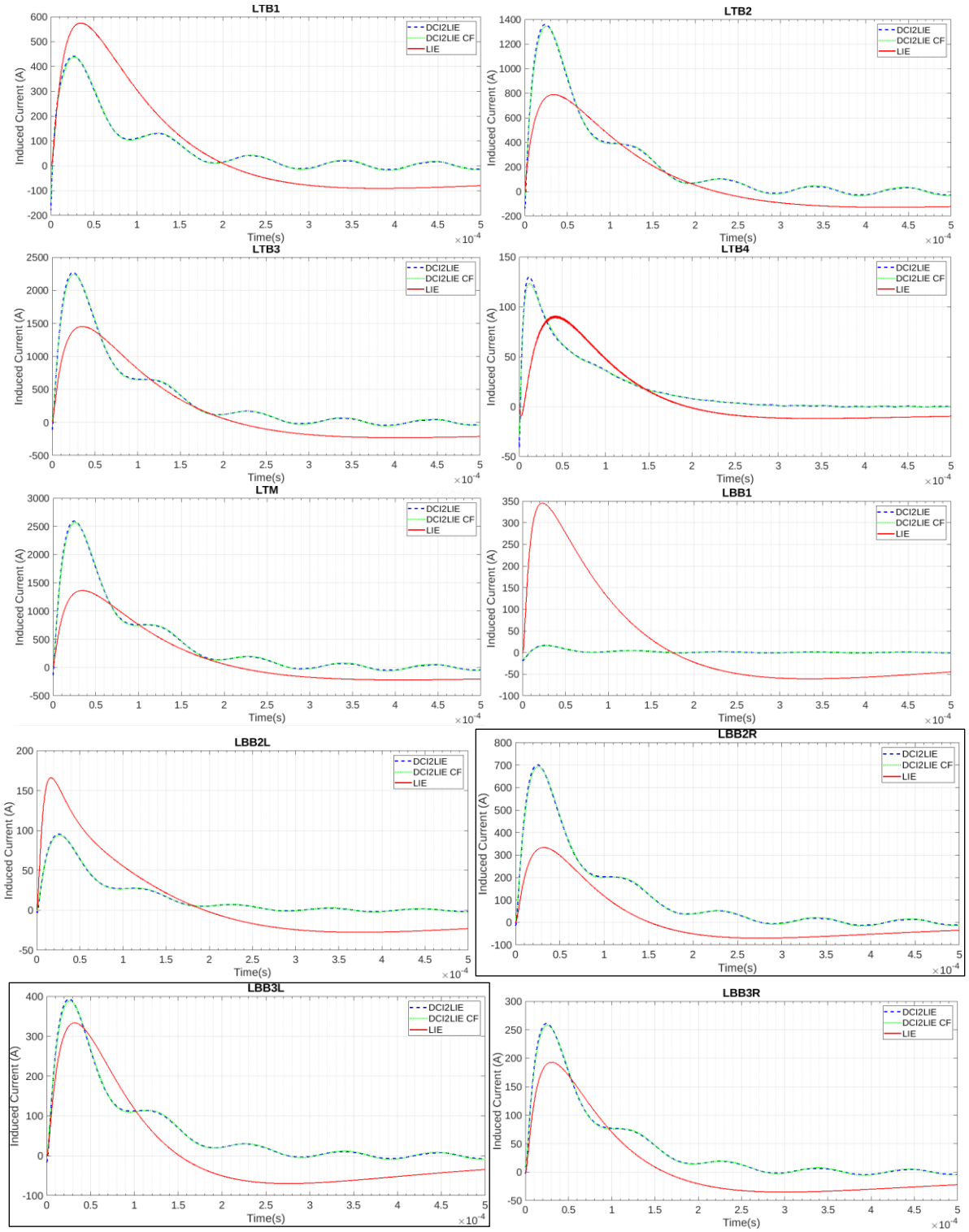

Fig. 5. Comparison of results (note that, for the sake of clarity, the color of the curves corresponds to the same color in the last line of the flowchart).

It is worth noting that results applying or not the correction factor are remarkably similar because in the testing campaign a cage return wire network according to the standards [2] and [3] was manufactured. That leads to a homogeneous current distribution and a correction factor near 1 for the lower frequency range (see Fig. 6). It was possible because of the size and shape of this test case but could be extremely complicated or even unaffordable for large aircrafts.

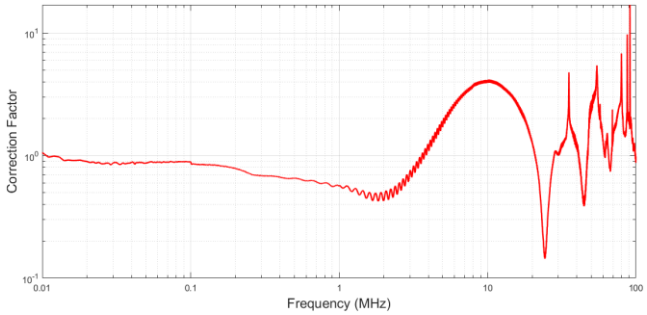

Fig. 6. Correction factor.

VII. APPROVAL CRITERION

An approval criterion based on waveform norms which define the main characteristics of the time domain response is established in order to compare curves in Fig. 5. In particular, we have chosen the peak amplitude, the time to peak, and the energy when the waveform has decayed to 50% of the peak value.

Additionally, a limit should be set for each one of the selected waveform norms. In order to do that, we are going to look at the measured curves (DCI2LIE or DCI2LIE CF of Fig. 5). The current induced on LBB2R and LBB3L should be the same because they are the two ends of a cable around 4 m long and lightning is a low frequency phenomenon for this length. Then, the approval criterion is established taken into account the difference between these two measurements, since we could not expect better agreement between simulated and measured results than between two measurements of the same observable.

Measurements in frequency domain for these two probes can be observed in Fig. 7. After executing the DCI post-process to these curves, they result in peak values of 693 and 389 A respectively (see Fig. 5). The difference between these two values is equivalent to 5.02 dB. Basically, this difference corresponds to the deviation between the two measured curves at low frequency (for instance, at 10 kHz it is 4.73 dB). In the same way, the energy up to 50% of the peak value is 17.92 and 5.62 J respectively, whose difference corresponds to 5.04 dB. Therefore, the approval criterion is set at 6 dB for the peak amplitude and the energy.

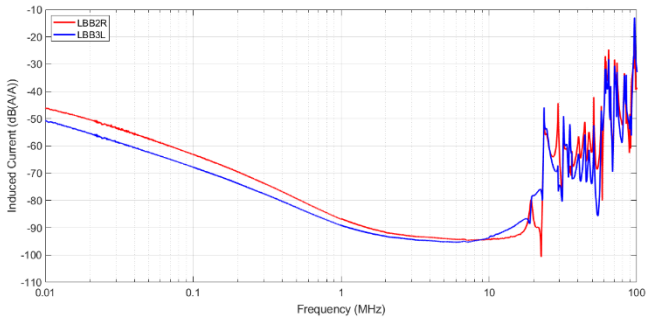

Fig. 7. Measurement comparison LBB2R versus LBB3L.

With respect to the time to peak, in an attempt to follow the same criterion, the limit has been chosen at 2, which means to double the time to peak, which corresponds to 6 dB.

This approval criterion will be shown by means of a color code, being green color for differences lower than 6 dB considered as good agreement, amber for differences between 6 and 10 dB considered as fair agreement, and red for differences higher than 10 dB considered as poor agreement.

VIII. VALIDATION

Table 1 shows the values of the mentioned waveform norms for each one of the ten cable current probes in both 'LIE' and 'DCI transformed to LIE' configurations, and the differences between them to assess the deviation. For peak amplitudes and energies, the differences are calculated in dB, whereas, for times to peak, the ratio between both times is calculated.

TABLE I
WAVEFORM NORMS COMPARISON

Probe	Test	Peak Amplitude (A)	Diff (dB)	Time to Peak (s)	Diff (us/us)	Energy 50% (J)	Diff (dB)
LTB1	DCI	438	-2,38	2,77E-05	1,27	7,32	-4,63
	LIE	575		3,52E-05		21,28	
LTB2	DCI	1344	4,61	2,53E-05	1,35	69,66	2,01
	LIE	790		3,41E-05		43,83	
LTB3	DCI	2241	3,75	2,54E-05	1,37	190,54	1,26
	LIE	1454		3,47E-05		142,44	
LTB4	DCI	123	2,62	1,17E-05	3,58	0,44	-0,52
	LIE	91		4,19E-05		0,49	
LTM	DCI	2566	5,47	2,58E-05	1,33	251,72	2,99
	LIE	1366		3,43E-05		126,31	
LBB1	DCI	16	-26,57	2,81E-05	1,23	0,00	-38,64
	LIE	346		2,28E-05		6,03	
LBB2L	DCI	94	-4,93	2,64E-05	1,64	0,33	-5,16
	LIE	166		1,61E-05		1,08	
LBB2R	DCI	693	6,34	2,57E-05	1,23	17,92	4,83
	LIE	334		3,17E-05		5,90	
LBB3L	DCI	389	1,33	2,65E-05	1,20	5,62	-0,21
	LIE	334		3,17E-05		5,90	
LBB3R	DCI	258	2,51	2,56E-05	1,18	2,53	1,07
	LIE	193		3,01E-05		1,98	

Regarding the peak amplitude, only one among the ten probes

gives bad results (LBB1). It belongs to the bottom harness. We have employed simulations to try to find the reason for this higher deviation. Making use of simulations we can visualize the current evolution by extracting images or even animations, which are helpful to analyze this kind of issues.

In this case, we have drawn snapshots of the current distribution at around 6.5 us, which is the time to the WFA peak and is around the time to peak of the surface current density wave shapes. The upper picture of Fig. 8 corresponds to LIE configuration (exciting the model with a WFA), whereas, on the lower picture, a DCI simulation, with the cage return wire network, is represented (also WFA has been used as wave shape of illumination to be able to compare the surface current distribution at the same temporal instant, but this time in a thin-wire voltage source used to excite the cage return).

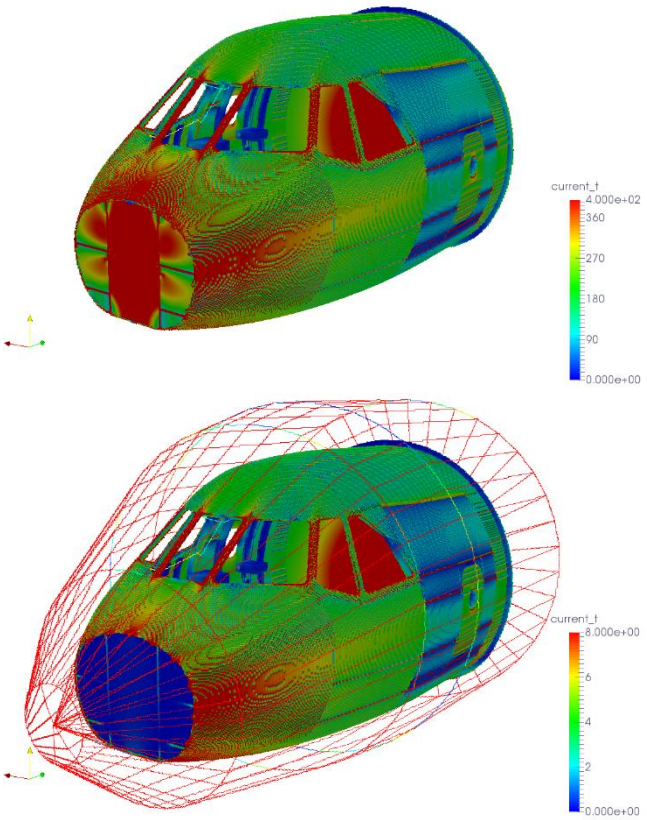

Fig. 8. Snapshot of the cockpit current distribution during lightning event (upper picture) and DCI test (lower picture).

In general, the current distribution is very similar in both configurations. However, there is a difference on the first frame. As it can be observed, the first frame is mostly in red color for LIE configuration because lightning impact has been attached to the center of this frame. By contrast, in DCI configuration, the injection has been performed through sixteen attachment points symmetrically distributed on the first frame boundary, and then the current flows along the cockpit while the first frame remains in blue color. Cable branch LBB1 is connected to a box which is just behind the first frame of the cockpit. Therefore, it receives a significant current injection in LIE configuration and hardly receives current in DCI configuration. Thus, the reason for the deviation is a difference in the surface current distribution on the cockpit for LIE and DCI configurations.

Continuing with the peak amplitude, one probe presents a deviation slightly higher than the 6 dB of margin (LBB2R), while four probes present an agreement within 3 dB of margin, which in terms of current means a deviation of only $\sqrt{2}$, value typically acceptable in EMC.

Regarding the time to peak, the probes exhibit very small differences except only one probe which presents a deviation that exceeds the double of the time to peak.

Regarding the energy, as it happens with the peak amplitude, only one out of the ten probes presents poor matching. The reason is the different drop slope shown by the two kinds of calculations, but also the difference in the peak amplitude which is again taken into account in the energy values. There are three probes which present an agreement between 3 and 6 dB of margin, and other six probes present an agreement with less than 3 dB of margin.

The presented validation results prove the validity of these lightning simulations within the established margin of 6 dB. The higher deviation found can be explained by the differences between a real lightning configuration and the DCI setup. Lightning simulations performed with representative EM models can be reliably used from the earlier stages of a project, predicting which routes could cause excessive levels of induced currents or voltages, and, consequently, equipment damage or malfunction. With this information at hand, appropriate solutions can be implemented in these earlier stages of the design, for instance, redefining the cable route or protecting the cable within adequate shielding.

IX. CONCLUSIONS

This paper is aimed to demonstrate the feasibility and reliability of lightning simulations. To this end, their results are compared with the ones coming from a standardized test used for lightning, the low-level DCI. This measurement technique is applied in frequency domain and on-ground, and, therefore, the results should be post-processed to obtain the time domain response to a full lightning threat.

The validation shown in this paper has been performed on a hybrid metal-composite and equipped aircraft cockpit and presents good agreement in the three main waveform characteristics analyzed. Making use of the capacity of the simulations to visualize the development of the lightning event, the main deviation found has been explained by a different surface current distribution between LIE and DCI configurations. Hence, these lightning simulation results can be considered valid within the applicable margins.

In accordance with the behavior observed in this particular set-up, we can conclude that, when carrying out a DCI technique, it must be taken into account that no artificial zones with very low field values are created by symmetric injection points or any other casuistry. For certification purposes, several configurations, not only for covering different zones in the aircraft, but also for searching maximums, must be tested, or

simulations can be used as well to support the process.

In the present study, two over-braided harnesses have been analyzed. A similar kind of analysis could be performed for not over-braided cabling, thus with point-to-point connections.

Moreover, lightning simulations not only show interesting results from an engineering point of view but are also aligned with the digitalization of processes and cost reduction of product development. Results can be obtained from the earlier stages of proof of concept and design of an aircraft, predicting the behavior of the object, and providing guidance on the decisions to be made to maximize the effectiveness of the protections. In a subsequent phase, simulations can be used to support the certification process, with the potential benefit of improving the aircraft safety by predicting the behavior of the object in configurations which could not be addressed by test and by checking a larger number of probes and even putting them in areas inaccessible for a measurement. In addition, sensibility analysis can be easily performed by simulations to evaluate the product variability according to the tolerances in different parameters. Finally, during the whole aircraft life until its end of service, time of aircraft testing can be saved using simulations to support aircraft maintainability or modifications.

REFERENCES

[1] EUROCAE ED-158, April 2020/SAE ARP5415, rev B, March 2020, "User's Manual for Certification of Aircraft Electrical/Electronic Systems for the Indirect Effects of Lightning".
[2] EUROCAE ED-105, rev A, Jul. 2013/SAE ARP 5416, rev A, Jan. 2013, "Aircraft lightning test methods".
[3] EUROCAE ED-107, rev A, Jul. 2010/SAE ARP 5583, rev A, Jun. 2010, "Guide to certification of aircraft in a high-intensity radiated field (HIRF) environment".
[4] Gil, E. P., G. G. Gutierrez, and R. M. Castejón, "Application of advanced simulations in time domain in the EMC certification process of an aircraft," Proceedings XXXIII URSI Symposium, Granada, Spain, 2018.
[5] PASSARO, http://passaro.inegi.up.pt/index.asp.
[6] Clean Sky 2, https://www.cleansky.eu/innovative-technologies-0.
[7] Guadalupe Gutierrez Gutierrez, Tim McDonald, Carlos Rodriguez Paños, Raul Molero Castejon, Hugo Tavares, Hirahi Galindo Perez, and Enrique Pascual-Gil, "Predictive Capacity of FDTD Method Embedding MTLN Technique for Lightning and HIRF Threats," Progress In Electromagnetics Research C, Vol. 107, 33-47, 2021.
[8] Pérez, F. C., G. Gutierrez Gutierrez, H. Tavares, A. Khamlichi, J. M. Alberquilla, R. Molero Castejón, N. Matos, and A. R. Linares, "Lightning low level vs high level direct current injection tests on a full scale aircraft cockpit," 2019 International Symposium on Electromagnetic Compatibility - EMC EUROPE, 644-649, Sep. 2019.
[9] Airbus Defence and Space, https://www.airbus.com/defence.html.
[10] CATIA by Dassault Systemes, http://www.3ds.com.
[11] Gutiérrez, G. G., E. P. Gil, D. G. Gómez, and J. I. P. Gómez, "Finite-difference time-domain method applied to lightning simulation and aircraft certification process," International Symposium on Electromagnetic Compatibility EMC Europe, York, UK, 2011.
[12] Gil, E. P., and G. G. Gutierrez, "Simplification and cleaning of complex CAD models for EMC simulations," International Symposium on Electromagnetic Compatibility EMC Europe, York, UK, 2011.
[13] Gutierrez, G. G., S. F. Romero, M. Gonzaga, E. Pascual-Gil, L. D. Angulo, M. R. Cabello, and S. G. Garcia, "Influence of geometric simplifications on lightning strike simulations," Progress In Electromagnetics Research C, Vol. 83, 15-32, 2018.
[14] Gutierrez, G. G., S. F. Romero, M. Gonzaga, E. Pascual-Gil, L. D. Angulo, M. R. Cabello, and S. G. Garcia, "Influence of geometric simplifications on high-intensity radiated field simulations," Progress In Electromagnetics Research C, Vol. 86, 217-232, 2018.
[15] Han, Dutton, Fan, "Model dispersive media in finite-difference time-domain method with complex-conjugate pole-residue pairs," IEEE Microwave and Wireless Components Letters, March, 2006.
[16] B. Gustavsen, "Improving the pole relocating properties of vector fitting," in IEEE Transactions on Power Delivery, vol. 21, no. 3, pp. 1587-1592, July 2006.
[17] Taflove, A. and S. C. Hagness, Computational Electrodynamics: The Finite-difference Time-domain Method, 3rd Edition, Artech House, Boston, 2005.
[18] S. G. Garcia, J. Alvarez, L. D. Angulo, and M. R. Cabello, "UGRFDTD EM solver," http://www.sembahome.org/.
[19] M. Cabello et al, "Numerical Assessment in Aeronautics for Electromagnetic Environmental Effects" in Electromagnetic Compatibility for Space Systems Design, IGI Global, 2018.
[20] Yee, K., "Numerical solution of initial boundary value problems involving maxwell's equations in isotropic media," IEEE Transactions on Antennas and Propagation, Vol. 14, No. 3, 302-307, 1966.
[21] Yik-Kiong Hue, F. L. Teixeira, L. S. Martin, and M. S. Bittar, "Three-dimensional simulation of eccentric LWD tool response in boreholes through dipping formations," in IEEE Transactions on Geoscience and Remote Sensing, vol. 43, no. 2, pp. 257-268, Feb. 2005, doi: 10.1109/TGRS.2004.841354.
[22] R. Holland, "Finite-difference time-domain (FDTD) analysis of magnetic diffusion," IEEE Trans. Electromagn. Compat., vol. 36, no. 1, pp. 32–39, Feb. 1994.
[23] Ruiz-Cabello N M, Abaļenkovs M, Diaz Angulo LM, Cobos Sanchez C, Moglie F, Garcia SG, "Performance of parallel FDTD method for shared- and distributed-memory architectures: Application to bioelectromagnetics," PLOS One, 15(9):e0238115, 11 Sep 2020.
[24] G. Junkin, "Conformal FDTD Modeling of Imperfect Conductors at Millimeter Wave Bands," in IEEE Transactions on Antennas and Propagation, vol. 59, no. 1, pp. 199-205, Jan. 2011, doi: 10.1109/TAP.2010.2090490.
[25] Cabello M. R., Angulo L., Alvarez J., I. D. Flintoft, Bourke S., Dawson J. F., Gómez Martín R. & G. Garcia S., "A Hybrid Crank Nicolson FDTD Subgridding Boundary Condition for Lossy Thin-Layer Modeling," IEEE Transactions on Microwave Theory and Techniques 65, 1397-1406, May, 2017.
[26] R. Holland and L. Simpson, "Finite-difference analysis of EMP coupling to thin struts and wires," IEEE Trans. Electromagnetic Compatibility, vol. EMC-23, no. 2, pp. 88–97, May 1981.
[27] Mur, Gerrit, "Absorbing boundary conditions for the finite difference approximation of the time-domain electromagnetic field equations," Electromagnetic Compatibility, IEEE Transactions on, vol. 23, issue 4, pp. 377-382, 1981.
[28] GiD, https://www.gidhome.com/.
[29] Dey, S., Mittra, R., "A locally conformal finite-difference time-domain (FDTD) algorithm for modelling three-dimensional perfectly conducting objects," IEEE Microwave and Guided Wave Letters, 7(9), 273-275, 1997.
[30] Cabello, M. R., Angulo, L. D. , Alvarez, J. , Bretones, A. R., Gutierrez, G. G., Garcia S. G., "A New Efficient and Stable 3D Conformal FDTD," IEEE Microwave and Wireless Components Letters, 26, 553-555, August, 2015.
[31] HIRF-SE project European Commission, December 2008 – May 2013, http://www.hirf-se.eu.
[32] Gutierrez, G. G., J. Alvarez, E. Pascual-Gil, M. Bandinelli, R. Guidi, V. Martorelli, M. F. Pantoja, M. R. Cabello, and S. G. Garcia, "HIRF virtual testing on the C-295 aircraft: on the application of a pass/fail criterion and the FSV method," IEEE Transactions on Electromagnetic Compatibility, Vol. 56, No. 4, 854-863, 2014.
[33] G. G. Gutierrez, D. M. Romero, M. R. Cabello, E. Pascual-Gil, L. D. Angulo, and S. G. Garcia, "On the Design of Aircraft Electrical Structure Networks," IEEE Transactions on Electromagnetic Compatibility, vol. 2, no. 58, pp. 401–408, 2016.
[34] G. G. Gutierrez, S. F. Romero, J. Alvarez, S. G. Garcia, and E. P. Gil, "On the use of FDTD for HIRF Validation and Certification," PIERS Progress In Electromagnetics Research Letters, vol. 32, pp. 145–156, 2012.
[35] Cabello, M. R., S. Fernández, M. Pous, E. Pascual-Gil, L. D. Angulo, P. López, P. J. Riu, G. G. Gutierrez, D. Mateos, D. Poyatos, M. Fernandez, J. Alvarez, M. F. Pantoja, M. Añón, F. Silva, A. R. Bretones, R. Trallero, L. Nu no, D. Escot, R. G. Martin, and S. G. Garcia, "SIVA UAV: A case study for the EMC analysis of composite air vehicles," IEEE Transactions on Electromagnetic Compatibility, Vol. 59, 1103-1113, Aug. 2017.

[36] Romero, S. F., G. G. Gutierrez, A. L. Morales, and M. A. Cancela, "Validation procedure of low level coupling tests on real aircraft structure," International Symposium on Electromagnetic Compatibility EMC, Europe, 2012.

[37] EUROCAE ED-84, rev A, July 2013/SAE ARP5412, rev B, January 2013, "Aircraft Lightning Environment and Related Test Waveforms".

[38] A. M. Wellington, "Direct current injection as a method of simulating high intensity radiated fields (HIRF)," IEE Colloquium on EMC Testing for Conducted Mechanisms, 1996, pp. 4/1-4/6, doi: 10.1049/ic:19960731.

[39] G. D. M. Barber, "The use of direct current injection (DCI) techniques for aircraft clearance," 10th International Conference on Electromagnetic Compatibility, 1997. (Conf. Publ. No. 445), 1997, pp. 199-204, doi: 10.1049/cp: 19971144.

[40] G. A. Rasek and S. E. Loos, "Correlation of Direct Current Injection (DCI) and Free-Field Illumination for HIRF Certification," in IEEE Transactions on Electromagnetic Compatibility, vol. 50, no. 3, pp. 499-503, Aug. 2008, doi: 10.1109/TEMC.2008.926872.

[41] Rasek, G. A., E. Pascual-Gil, A. Schröder, I. Junqua, R. Guidi, C. A. Kreller, H. Brüns, and S. E. Loos, "HIRF transfer functions of a fuselage model: Measurements and simulations," IEEE Transactions on Electromagnetic Compatibility, Vol. 56, 311-319, Apr. 2014.

[42] Rasek, G. A., A. SchrÄoder, P. Tobola, Z. ·Reznícek, S. E. Loos, T. Tischler, and H. Brüns, "HIRF transfer function observations: Notes on results versus requirements and certification approach," IEEE Transactions on Electromagnetic Compatibility, Vol. 57, No. 2, 195-202, 2015.

[43] J. Ückerseifer, M. Aidam, M. Rothenhäusler and F. Gronwald, "A Numerical Analysis of HIRF- and DCI-Equivalence by Characteristic Mode Theory," 2019 International Symposium on Electromagnetic Compatibility - EMC EUROPE, 2019, pp. 315-320, doi: 10.1109/EMCEurope.2019.8871548.

[44] Bastard, C., M. Meyer, C. Guiffaut, and A. Reineix, "Ways of improvement for HIRF transfer function assessment on rotorcraft," 2019 ESA Workshop on Aerospace EMC, 1-6, May 2019.